Biomimetic Micromechanical Adaptive Flow-Sensor Arrays

Gijs Krijnen[*], Arjan Floris, Marcel Dijkstra, Theo Lammerink, Remco Wiegerink
Transducers Science & Technology group, MESA+ Research Institute
Univeristy of Twente, p.o. box 217 7500 AE Enschede, The Netherlands

ABSTRACT

We report current developments in biomimetic flow-sensors based on flow sensitive mechano-sensors of crickets. Crickets have one form of acoustic sensing evolved in the form of mechanoreceptive sensory hairs. These filiform hairs are highly perceptive to low-frequency sound with energy sensitivities close to thermal threshold. In this work we describe hair-sensors fabricated by a combination of sacrificial poly-silicon technology, to form silicon-nitride suspended membranes, and SU8 polymer processing for fabrication of hairs with diameters of about 50 μm and up to 1 mm length. The membranes have thin chromium electrodes on top forming variable capacitors with the substrate that allow for capacitive read-out. Previously these sensors have been shown to exhibit acoustic sensitivity. Like for the crickets, the MEMS hair-sensors are positioned on elongated structures, resembling the cercus of crickets. In this work we present optical measurements on acoustically and electrostatically excited hair-sensors. We present adaptive control of flow-sensitivity and resonance frequency by electrostatic spring stiffness softening. Experimental data and simple analytical models derived from transduction theory are shown to exhibit good correspondence, both confirming theory and the applicability of the presented approach towards adaptation.

Keywords: biomimetics, MEMS, flow-sensors, mechano-sensory hairs, adaptation, spring-softening, drag-force, capacitive sensing.

1. INTRODUCTION[†]

Sensory systems in biology are among the most sensitive and evolved known to man. In comparing biological and engineered systems for similar functions one often finds striking differences in implementation; for example when taking a look at auditory sensing. 1) In biological systems sensing elements are based on the flow-sensitivity of large arrays of parallel operating mechano-sensors (hairs, cilia). 2) Biological systems rely heavily on mechanical filtering and amplification. And 3) noise may play a beneficial role when perceiving signals near the noise limits. Engineered systems for acoustic sensing on the other hand are based on pressure measurements using single moving structures (e.g. membranes as in microphones), perform filtering and amplification in the electronic domain (in a sequential manner), and generally see their usable dynamic sensing range being limited by noise. An example of mechanical filtering in biology is found in the auditory system of mammals where tapered "sound-board" like resonator structures (basilar membrane) with complex interacting inner- and outer- hair-cells perform distributed filtering, amplification and adaptation in the mechanical domain [2]. At the same time parallelism helps to overcome constraints of bandwidth of the neural systems and provides robustness, redundancy and gradual decline. Examples of how biological systems benefit from noise are seen in the form of stochastic resonance and amplification [3] as observed in crickets [4] and crayfish [5].

Despite the advancement of mankind in many areas of technology it is still challenging for engineered systems to compete with biological systems. For example: the auditory capabilities of bats to perceive their environment, locate prey and to navigate at high velocities through complex surrounding (e.g. with leafed brushes and trees) has no manmade equivalent. Likewise the sensitivity of hair-based acoustic mechano-sensors, found on insects [6], to perceive acoustic signals at thermal noise levels is astounding. It is this kind of performance that raises interest in biological systems with the purpose to improve engineered systems and gain extended functionality.

---

[*] Corresponding author email: g.j.m.krijnen@ewi.utwente.nl, phone: x31-53-4894422, fax: x31-53-4893343
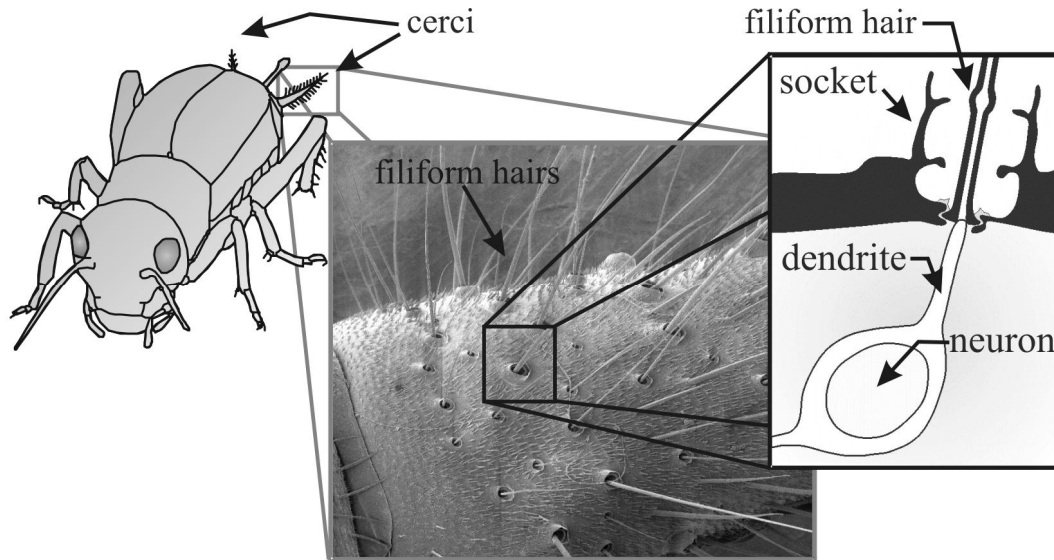[†] The introductory part of this contribution has been adapted from [1].

Fig. 1. Filiform hairs on the cerci of crickets [8].Centre image: SEM picture of part of a cercus, courtesy by Jerome Casas, IRBI, Université de Tours.

Crickets have achieved acoustic sensing by evolving sensitive mechano-receptive sensory hairs. These so-called filiform hairs are highly perceptive to low-frequency sound with energy sensitivities below thermal threshold [6]. The sensory hairs of the cricket are situated on the back of the body on appendices called cerci. Depending on species, the hairs of adults vary in length up to around 1.5 mm. For some species a bimodal distribution is found with concentrations around 150 μm and 750 μm [7]. Each hair is lodged in a socket, guiding the hair to move in a preferred direction. The hair is held in its socket by an elastic material surrounding the base. Airflow causes a neuron to fire, by rotation of the hair base (figure 1). Depending on hair-length and frequency sensitivities can be down to 10's of μm/s flow velocity amplitude [6]. Crickets are able to pinpoint low-frequency sound from any given direction using the combined neural information of all sensory hairs [8].

It is interesting to note that crickets have developed flow sensitive hairs rather than pressure sensitive sensors. As Tautz has pointed out [9] this is more or less a necessity since important predators of crickets, such as wasps and spiders, are too small to produce any significant pressure variations at the important frequencies of e.g. wing beats (tens to hundreds of Hz). This observation is based on the fact that substantial pressure waves can only be emitted by moving bodies larger than $\approx 2\pi\lambda$, with λ the wavelength of the sound. Moreover, many attacks on crickets will take place at relative short distances such that the cricket may be considered in the near field of the sound producing predator, i.e. where particle velocity is more readily conceivable than pressure fluctuations.

There seems to be a favourable size match between the primary sensing parts (e.g. mechano-sensing hairs found on cricket cerci with lengths roughly between $100 - 1000$ μm) and what can be made by a technology generally denoted by "Micro Electro Mechanical Systems" (MEMS). It allows, in principle, for bio-mimicking of biological sensory systems such as the flow sensitive hairs of cricket, the tactile hair sensors on spiders [10], the lateral line sense organs of fish [11] and the mammalian cochlea [2]. Mimicking the cricket flow-sensitive hairs is not necessarily suggested only by flow-sensitivities; whereas the crickets' flow-sensors are amongst the most energy-sensitive sensors known, this does not automatically translate into the lowest flow-velocity sensitivities. E.g. an engineered hot-wire anemometer based particle velocity sensor like the MicroFlown [12] is able to sense flows as small as 10's of nm/s but only doing so by utilising a dissipative modulation type of sensing using 10s of mW of power. What makes drag-torque based flow-sensors very interesting is the ability to arrange them in densely packed arrays allowing for the determination of flow-patterns rather than a flow measurement at a single point. Moreover, utilising variability in the sensors allows for frequency dependent responses much the same way mammalian ears function as a real-time Fourier transform. Additionally we will show that specific implementations of such sensors can be made adaptable with respect to sensitivity and resonance frequency whereas electro-mechanical signal processing, including parametric filtering and amplification belongs to the range of potentials of these devices.

2. ADAPTIVE DRAG-TORQUE SENSITIVE FLOW SENSORS

2.1 Operation principle

Artificial mechano-sensory hairs are based on the tilting of a membrane due to viscous drag. The membrane is suspended by torsion beams. In the sensors described here both the membrane and the torsion beams are made of silicon nitride. The membranes can have various forms, e.g. circular or rectangular. Chromium electrodes are deposited on top of the membrane. These electrodes form capacitors with the underlying common electrode formed by the highly doped silicon wafer. Due to the drag-induced torque the membranes tilt and therefore the capacitors on both halves of the sensor will show (opposite) change in capacitance. These changes in capacitance can be determined differentially and provide a means of measuring the tilting angle and, hence, the flow causing the tilt.
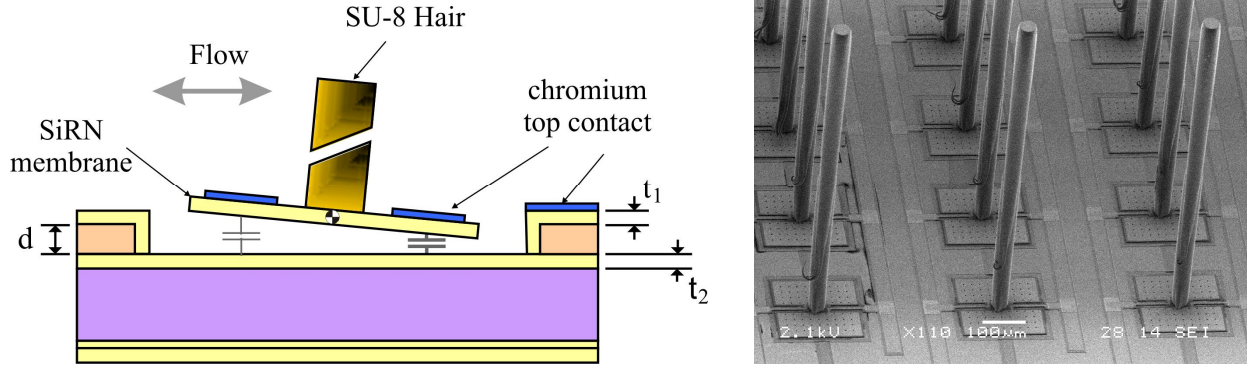

Fig. 2. Left: schematic representation of artificial biomimetic flow-sensors based on cricket mechano-sensory hairs. Right: Scanning Electron Microscope image of actual sensors. Note that the electrical connection to the top-electrodes on the membranes runs over the torsion beams.

2.2 Mechanical system

The mechanics of the sensory hairs of crickets has been modelled extensively [e.g. 13, 14]. Filiform hairs are described as an inverted pendulum, a second order mechanical system, determined by the torsional spring constant S, the moment of inertia J and the torsional resistance R. Conservation of angular momentum requires that

$$J\frac{d^2\alpha(t)}{dt^2} + R\frac{d\alpha(t)}{dt} + S\alpha(t) = T_{drag}(t) \tag{1}$$

where T_{drag} is the flow induced drag torque. Indicative values for cricket filiform hairs with a length of 1000 μm are: $S \approx 2.10^{-11}$ Nm/rad, $J \approx 5 \cdot 10^{-18}$ kg·m^2 and $R \approx 10^{-14}$ Nms/rad [13]. Resonance frequencies of filiform hairs are in the range of 100 to 3000 Hz depending on hair-length and structural allometric scaling. However, best frequencies are lower since the systems are moderately damped and have almost constant quality factor over the entire range of hair-length. The damping is hypothesised to have evolved under constraints of impedance matching to the mechanical impedance of the driving flow as given by the Stokes expressions [13]. Impedance matching allows for maximum energy transfer, hence optimised sensitivity of the sensory hairs.

For harmonic excitation torque at radial frequency ω the steady oscillatory hair movement $\alpha(\omega)$ can be described by the well-known complex amplitude function:

$$\alpha_0(\omega) = \frac{T_{d0}}{J} \cdot \frac{1}{\omega_0^2 - \omega^2 + j\omega(R/J)} \tag{2}$$

where T_{d0} is the amplitude of the drag-torque and ω_0 is the resonance frequency given by $(S/J)^{0.5}$.
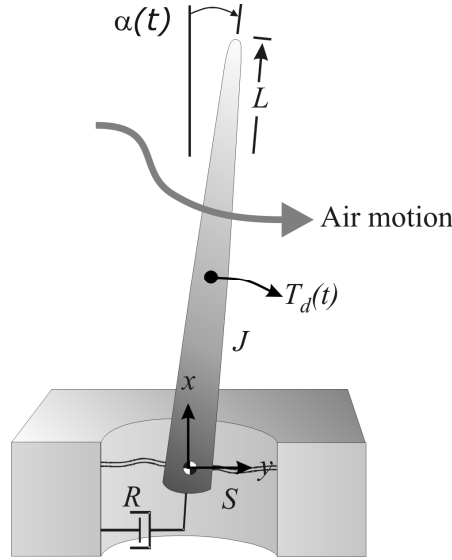
Fig. 3. Hairs can be modeled as an inverted pendulum representing a damped second order mechanical system (adapted from [14]).

2.3 Aerodynamic modeling

Here we will briefly reiterate the theoretical framework developed for the understanding of flow-sensitive mechano-sensors of crickets [13, 14] and apply it to our biomimetic sensors. The hairs are deflected by viscous drag on the hair shaft due to particle velocity. For harmonic flow velocities parallel to a flat surface given by a far-field of the form

$$v_{y,\infty}(t) = V_0 \cdot \sin(\omega t) \tag{3}$$

the frequency dependent velocity profile above the surface is given by [13, 14]:

$$v_y(x,t) = V_0 \cdot \sin(\omega t) - V_0 \cdot e^{-\beta x} \cdot \sin(\omega t - \beta x)$$

$$\beta = \sqrt{\frac{\omega}{2 \cdot \nu}} \tag{4}$$

with ν the kinematic viscosity, x the distance from the surface and ω the angular frequency of the harmonically oscillating flow. Due to viscosity and no-slip at the interface between fluid and fixed surface there is a transition zone between zero velocity and the far-field velocity, the so-called boundary layer. The boundary layer thickness (δ_b) depends on $2/\beta$, being larger at lower frequencies. Figure 3 shows calculated and measured normalised flow-profiles above flat surfaces for various time-instants of one period of oscillation. Agreement between both is excellent permitting to use equation (4) in further modelling approaches.

In the small Reynolds number regime the drag-forces can be described by the Stokes expressions. These state that the drag-force by a fluid-flow given by equation (3) on a cylinder of unit length is given by [13]:

$$F_d(t) = \left\{ 4\pi\mu \cdot \frac{-g}{g^2 + (\pi/4)^2} \right\} V_0 \cdot \sin(\omega t) + \omega \left\{ \pi\rho_a a^2 + \frac{4\pi\mu}{\omega} \cdot \frac{\pi/4}{g^2 + (\pi/4)^2} \right\} V_0 \cdot \cos(\omega t) \tag{5}$$

with μ the dynamic viscosity, a the radius of the cylinder and ρ_a the mass-density of air. The variable g is given by:

$$g = \ln\left(a\beta / \sqrt{2}\right) + \gamma \tag{6}$$
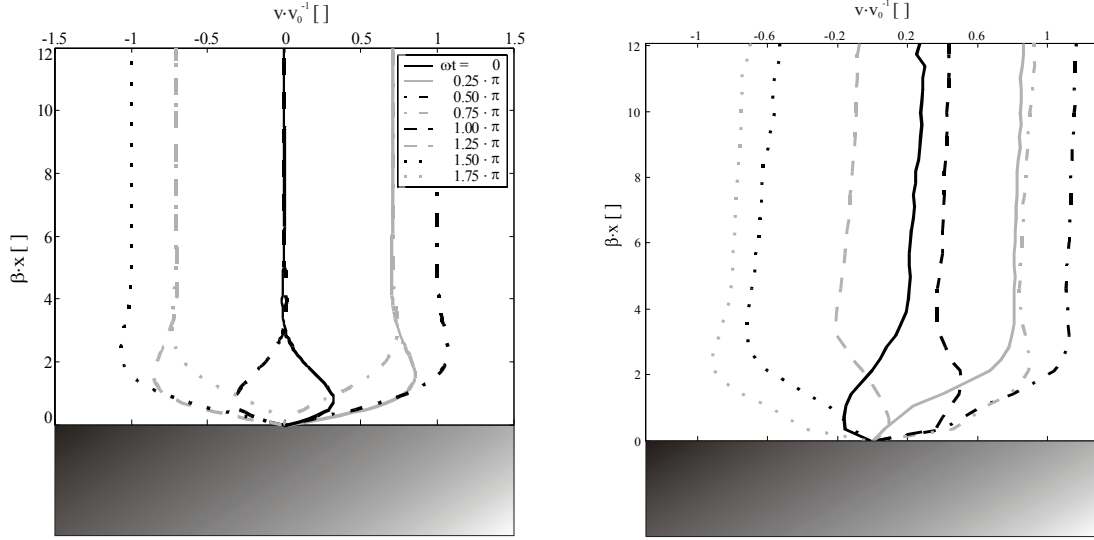
where γ is Euler's constant (0.5772..).

Fig. 4. Oscillating boundary layer on a flat surface, a) calculated, b) measured using a Particle Image Velocimetry setup, normalised with: $v_{air} = 1.79 \cdot 10^{-5}$ N·s·m^{-2} , $v_0 = 3$ cm·s^{-1} and $f = 60$ Hz.

The velocity in (5) is actually the velocity difference between the flow and the hair. However, the stiffness of our hairs is on the order of 10^{-8} Nm/rad and hair movement is relatively small in our structures so that the velocity difference can be approximated by the flow velocity itself (eq. 3). The total torque on the filiform hairs can be calculated by integrating the drag-moment along the hair:

$$T_d = \int_0^L F_d(x)x\,dx \qquad (7)$$

Using (4), (5) and (7) the total drag-torque on the hairs can be determined. The integration (equation 7) is readily done numerically.
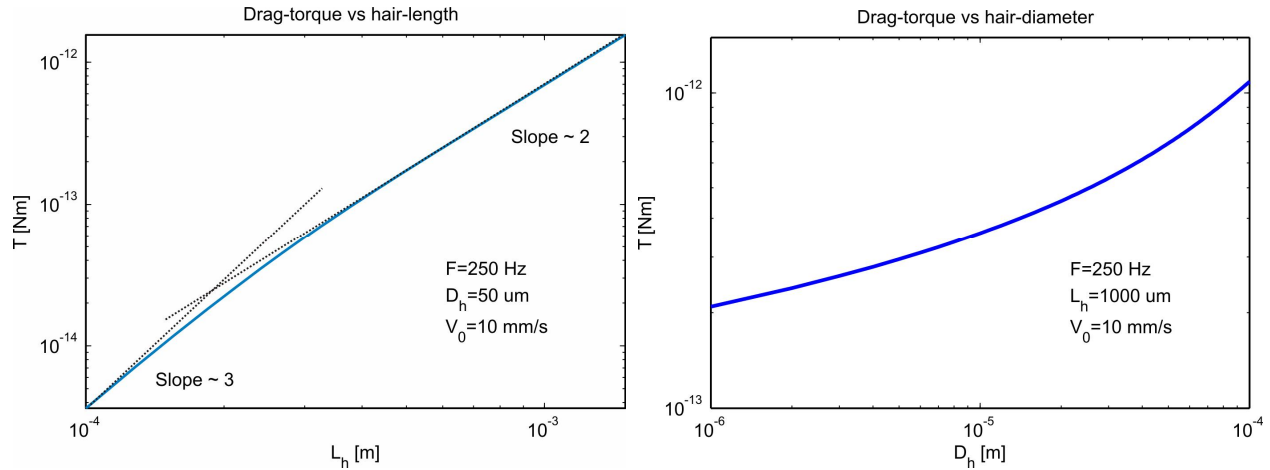

Fig. 5. Drag-torque predictions at 250 Hz. Left: Drag-torque acting on a cylinder of 50 μm diameter, as a function of hair length (model). Right: Drag-torque acting on a 1 mm long cylinder as a function of hair diameter.

The drag-torque increases roughly proportional to the hair length cubed L^3 when $L<2/\beta$ showing the importance of hair-length for optimised sensitivity (see figure 5). For a hair to effectively pick-up drag-torque it is essential that it extends out of the boundary layer. With a kinematic viscosity of $15.1 \cdot 10^{-6}$ m^2/s for air and at a frequency of 100 Hz this translates into a minimum hair-length of about 440 μm. For lower frequencies this length is even longer. Once the hair-length is

larger $L>2/\beta$ the drag-torque increases proportional to the length squared, as can be expected from the constant velocity amplitude (equation 4) and equations (5) and (7). The drag-torque amplitude of a 1 mm long, 50 μm diameter hair, exposed to a harmonic air flow of 250 Hz was calculated to be 6 10^{-11} Nm per m/s of flow-velocity amplitude as an indication of the torque-magnitude that can be expected. Varying the hair diameter is not dramatically affecting the drag-torque, especially not at low frequencies, as can be seen from figure 5 but also from equation (5).

2.4 Transducer modeling

The sensitivity (η) to measure drag-induced rotation is proportional to the change in capacitance per unit rotation. Since one half of the membrane moves upward and the other downward, the capacitance difference per unit of rotation can be calculated in the parallel plate approximation from:

$$\eta = 2 \cdot \frac{\partial C}{\partial \alpha}\bigg|_{\alpha=0} = 2 \cdot \lim_{\alpha \to 0} \frac{\partial}{\partial \alpha}\left(\int_A \frac{\varepsilon_0}{d_0 - \alpha y}\, dA\right) = 2 \cdot \int_A \lim_{\alpha \to 0}\left(\frac{\varepsilon_0 y}{(d_0 - y\alpha)^2}\right) dA = 2\varepsilon_0 \int_A \frac{y}{d_0^2}\, dA \qquad (8)$$

where use has been made of $\sin\alpha \approx \alpha$ for the small angles of rotation encountered, in which y is the distance to the rotation axis, A is the area of half of the membrane. The dielectric thickness d_0 is given by:

$$d_0 = d + \frac{t_1 + t_2}{\varepsilon_r} \qquad (9)$$

where ε_0 and ε_r are the dielectric constant of air and the relative dielectric constant of silicon nitride, respectively. For two semi-circular membranes the sensitivity is given by

$$\eta_C = 2\varepsilon_0 \int_0^\pi \int_0^R \frac{y}{d_0^2} r\, d\varphi dr = 2\varepsilon_0 \int_0^\pi \int_0^R \frac{r^2 \sin\varphi}{d_0^2}\, d\varphi dr = \frac{4\varepsilon_0}{3}\frac{R^3}{d_0^2} \qquad (10a)$$

with R the radius of the membrane. In case the membranes are subjected to stress and are (upward) curved up to a distance δ at the rim the expression becomes:

$$\eta_C = \frac{4\varepsilon_0}{3}\frac{R^3}{(d_0 + \delta)d_0} \qquad (10b)$$

For a sensor containing two rectangular membranes of width w and length l the sensitivity is:

$$\eta_R = 2\varepsilon_0 \int_0^w \int_0^l \frac{y}{d_0^2}\, dydz = \frac{\varepsilon_0 w l^2}{d_0^2} \qquad (11)$$

Sensors have been fabricated with circular as well as with rectangular membranes. Typically the gap between the electrodes (d) is 1 μm and the thickness of the silicon nitride layers t_1 and t_2 are 1 μm and 0.1 μm respectively. In case of circular membranes R is 100 μm giving a sensitivity of $\eta_C = 9.0$ pF/rad whereas in case of rectangular membranes $w = 200$ μm and $l = 100$ μm giving a sensitivity of $\eta_R = 15.4$ pF/rad.

2.5 Sensor response model

In general solving equations (1), (5) and (7) simultaneously under boundary conditions of the applied oscillatory flow (equation 4) requires integration in the time domain to account for relative flow velocities in dependence of the hair motions. However, in case of the artificial sensory hairs, with relative large rotational stiffness S and small rotations one may obtain the total mechanical sensor response from the multiplication of equations (2) and (7), basically taking T_d as an excitation independent of the mechanical response. Additionally, multiplying the mechanical response by η gives the total electro-mechanical sensitivity. The total response, including the mechanical response of the sensor, shows a band-pass behaviour. In crickets, the many cercal filiform hairs vary in their band-pass behaviour, because the mechanical

properties and drag-torque are dependent on the hair length. By combining many dissimilar filiform hairs the cricket is able to create a sensitive sensory system, which has a relatively balanced frequency spectrum [7].

2.6 Electrostatic spring softening by DC-biasing

Apart from enabling the measurement of the tilt-angles of the hair-sensor, the capacitive structures also allow for the application of electrostatic forces which can be used to adaptively change the effective properties of the sensors. When a DC-bias voltage is applied to both sides of a sensor that is not subjected to a flow, symmetry of the sensor will cause cancellation of the electrostatic torques. However, when the membranes are somewhat tilted, the side with the smallest gap will experience the largest electrostatic force. This results in an active contribution of the electrostatic forces to the total tilt of the membrane and effectively the system behaves as if it has a smaller torsional stiffness than the actual physical torsional stiffness in the system, i.e. electrostatic spring softening.
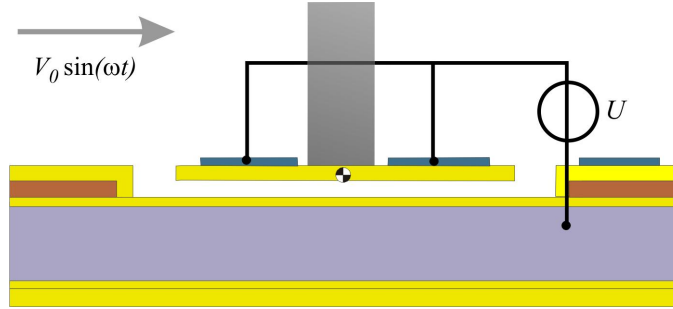

Fig. 6. Using a DC-bias the effective spring-stiffness of an artificial hair-sensor can be adaptively changed.

Transduction theory shows that the effective spring stiffness is given by:

$$S_{eff} = S - \frac{U^2}{2} \frac{\partial^2 C}{\partial \alpha^2} = S - U^2 \kappa \qquad (12)$$

Where S_{eff} is the effective spring constant, α is the membrane angular rotation, S is the physical rotational spring stiffness of the torsion beams, U is the applied bias voltage, C is the capacitance of the device and κ is the second derivative of the capacitance with respect to the angle of rotation divided by two. Since U^2 is positive an applied bias voltage will always give a reduction in the spring stiffness. At frequencies sufficiently lower than the resonance frequency the effective spring stiffness variations will allow for adaptive sensitivity variations according to:

$$\alpha_0 = \frac{T_{d0}(\omega, V_0)}{S_{eff}} = \frac{\alpha_{00}}{1 - \frac{\kappa}{S} U^2} \qquad (13)$$

Where T_{d0} is the amplitude of the drag torque on the hair (depending on frequency ω and far-field velocity amplitude V_0) and α_{00} is the amplitude of the angle of rotation for given T_{d0} without applied DC-bias. By the relation between resonance frequency and spring stiffness we expect a dependency of the resonance frequency, ω_0, on the DC-bias voltage according to:

$$\omega_0(U_{bias}) = \sqrt{\frac{S_{eff}(U)}{I}} = \omega_{00} \sqrt{1 - \frac{\kappa}{S} U^2} \qquad (14)$$

Here κ/S is a constant depending on the geometry of the structure and ω_{00} is the resonance frequency without applied bias voltage. From equations (2) and (3) it follows that the sensitivity and the resonance frequency of the sensors can be adaptively changed to accommodate optimal signal reception. Obviously, judging from equations (13) and (14) it can be seen that the biasing effects are dependent on the ratio κ/S. Moreover, equation (12) predicts that instability ($S_{eff} = 0$) will occur at a bias voltage U_i given by:

$$S_{eff} = 0 \Rightarrow U_i = \pm \sqrt{\frac{S}{\kappa}} \qquad (15)$$

In order to estimate the sensitivity to DC-biasing we calculated the coefficient κ. In General this coefficient cannot easily be calculated analytically for any non-zero α. However, in case of the hair sensors studied here, with small angles of rotation encountered in practice, κ is calculated from the parallel plate approximation as:

$$\kappa = \frac{\partial^2}{\partial \alpha^2} \left(\frac{1}{2} \int_A \frac{\varepsilon_0}{d_0 - y\alpha} dA \right) \Bigg|_{\alpha=0} \approx \lim_{\alpha \to 0} \frac{1}{2} \int_A \frac{\partial^2}{\partial \alpha^2} \left(\frac{\varepsilon_0}{d_0 - y\alpha} \right) dA = \lim_{\alpha \to 0} \frac{1}{2} \int_A \frac{\varepsilon_0 y^2}{(d_0 - y\alpha)^3} dA = \varepsilon_0 \int_A \frac{y^2}{d_0^3} dA \qquad (16)$$

where d_0 is the dielectric thickness as defined in equation (9) and A the surface area of the electrodes. Using equation (16) we find for a circular shaped membrane:

$$\kappa_C = 2\varepsilon_0 \int_0^R \int_0^\pi \frac{(r\sin\phi)^2}{d_0^3} r d\phi dr = \frac{\varepsilon_0}{4} \frac{\pi R^4}{d_0^3} \qquad (17a)$$

where R is the radius of the membranes. Due to stress-induced curvature of the membranes with maximum deflection δ at the rim equation (17) needs to be adjusted yielding approximately:

$$\kappa_C = \frac{\pi \varepsilon_0}{8\delta} R^4 \left\{ \frac{1}{d_0^2} - \frac{1}{(d_0 + \delta)^2} \right\} \qquad (17b)$$

2.7 Performance predictions

Using the various relations derived above model predictions can be made regarding the sensor performance. Geometric and other values are listed in table 1. Comparing artificial hair-sensors with cricket sensory hairs of about 1 mm length it is interesting to note that a) the stiffness of the MEMS sensors is about 360 times higher than that of the crickets and b) the moment of inertia is about 150 times larger. This translates into a 360 times smaller sensitivity and about 1.6 times higher resonance frequency.

Table 1. Sensor dimensions and material properties used for the model predictions

Membrane (SiRN)		Springs (SiRN)		Hairs (SU-8)	
Diameter	210 μm	Length	75 μm	Length	980 μm
Thickness	0.9 μm	Width	10 μm	Diameter	50 μm
Gap spacing	1 μm	Thickness	0.9 μm	Mass density	1200 kg/m^3
Curvature δ	2.0 μm	Youngs Modulus	310 GPa		
Diameter electrodes	200 μm	Poisson ratio	0.24		
ε_r	7.5				
Sensitivity η_C	1.39 pF/rad	Rotational stiffness S	7.2·10^{-9} Nm/rad	Moment of inertia	0.744·10^{-15} kg·m^2
Biasing κ_C	0.11·10^{-9} Nm/rad·V^2	κ_C/S	15.6·10^{-3} V^{-2}	Resonance frequency	496 Hz

Figure 7 shows various curves for a range of bias voltages between 1.4 V (red curve) and 7.2 V (green curve). Since the mechanical model does not include any physical damping, e.g. such as squeezed film effects, the damping coefficient R has been set to produce a quality factor $Q=2$ at zero bias-voltage and kept constant for the other curves. This results in a decrease of quality factor with increasing bias-voltage (decreasing resonance frequency). The model shows the increase in sensitivity and decrease in resonance frequency according to the equations (13) and (14) respectively with κ taken as given in table 1. The predicted bias-voltage resulting in instability (U_i) in this situation is about 8 V. Predicted

sensitivities are on the order of 10 – 100 fF·s/m and these values can be scaled up linearly with the number of hair-sensor in parallel.
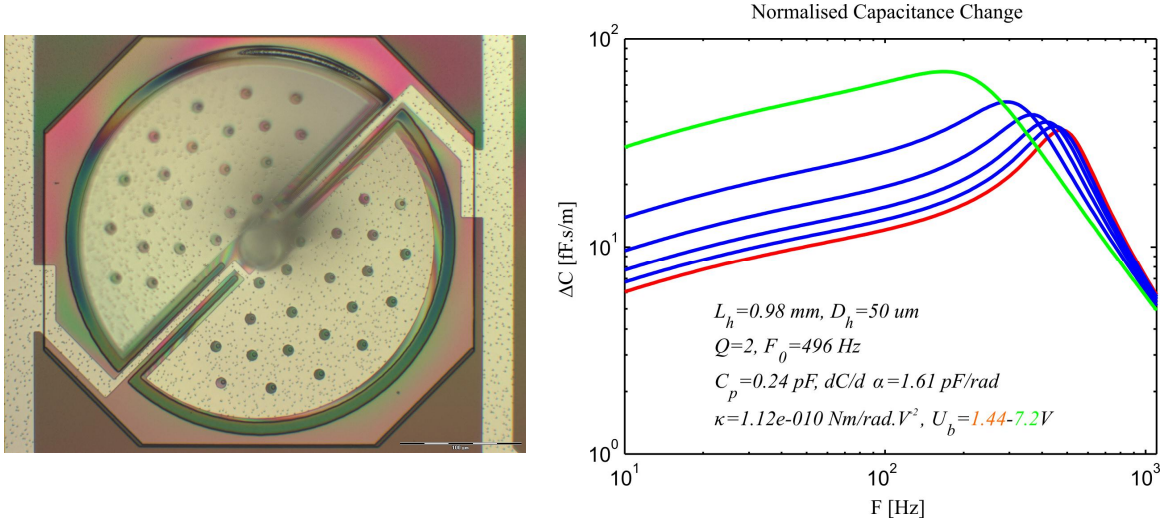

Fig. 7. Left: top-view of a realized circular sensor with dimensions as used for the modelling. Right: Sensor-response model-predictions including the effect of electrostatic spring softening.

2.8 Figure of merit and optimization

Using the model we investigated the dependence of the sensitivity as a function of hair-length (see figure 5). The drag-torque increases approximately proportional to the hair length cubed $(L_h)^3$, when L_h is smaller than the boundary layer thickness (δ_b) and with approximately $(L_h)^2$ when $L_h > \delta_b$. Changing the diameter of the hairs (figure 5) is by far not as influential. Although depending on frequency, in the frequency range of interest the relation between the drag-torque and the diameters can be approximated by $\propto (D_h)^{1/3}$.

Sensor-optimisation has two dimensions: usable bandwidth and (low-frequency) sensitivity. If one of both is (too) low the usability of the sensor is strongly hampered. Therefore we define a figure of merit (FOM) as the product of usable bandwidth (i.e. resonance frequency) and sensitivity (i.e. the drag-torque to which a hair is exposed) yielding:

$$FOM \equiv \omega_0 \cdot \frac{T_d}{S} = \sqrt{\frac{S}{J}} \cdot \frac{T_d}{S} \propto \sqrt{\frac{S}{\rho L_h^3 D_h^2}} \cdot \frac{L_h^2 D_h^{1/3}}{S} = \sqrt{\frac{L_h}{\rho S D_h^{4/3}}} \tag{18}$$

This FOM shows that sensitive sensors with a usable bandwidth should have long, thin hairs made of low density material, and small torsion stiffness, exactly what is seen in nature. In comparing the FOM of the artificial hair-sensors to the FOM of the crickets' hair-sensors, we find that the ratio is about 96 for hairs of 1 mm length. Crickets out-perform artificial sensors because of their low torsional stiffness ($2 \cdot 10^{-11}$ vs. $7 \cdot 10^{-9}$ Nm/rad) and small average hair-diameter (4.5 vs. 50 μm) giving clear directions for further optimisation.

3. FABRICATION

In this work hair-sensors are fabricated by a combination of a sacrificial poly-silicon technology, to form silicon-nitride suspended membranes, and SU-8 polymer processing for hair fabrication. A condensed fabrication scheme is shown in Figure 7.

Processing starts with a highly conductive silicon wafer, since the substrate is used as a common electrode for capacitive read-out (a). A 100 nm thin low-stress silicon-rich-nitride (SRN) layer is deposited by LPCVD [15], for the protection of the substrate during later etching of the sacrificial layer (b). Subsequently a Vangbo mask is applied in the SRN on the back-side to determine the crystallographic directions with great accuracy, needed for the later etching of precisely aligned V-grooves by KOH-etching (c). A 1 μm sacrificial poly-silicon layer is deposited by LPCVD (d) and patterned to form etch-stop trenches on the top side and removed from the back-side (e). A second, 1 μm thick SRN layer is

deposited (f), followed by sputtering (g) and structuring (h) of a 20 nm chromium layer. The SRN layer on the back-side is patterned and used to etch V-grooves by anisotropic KOH etching (i). The width of the grooves is chosen such that the V-grooves end to a distance of about 50 μm from the top-side maintaining structural integrity.
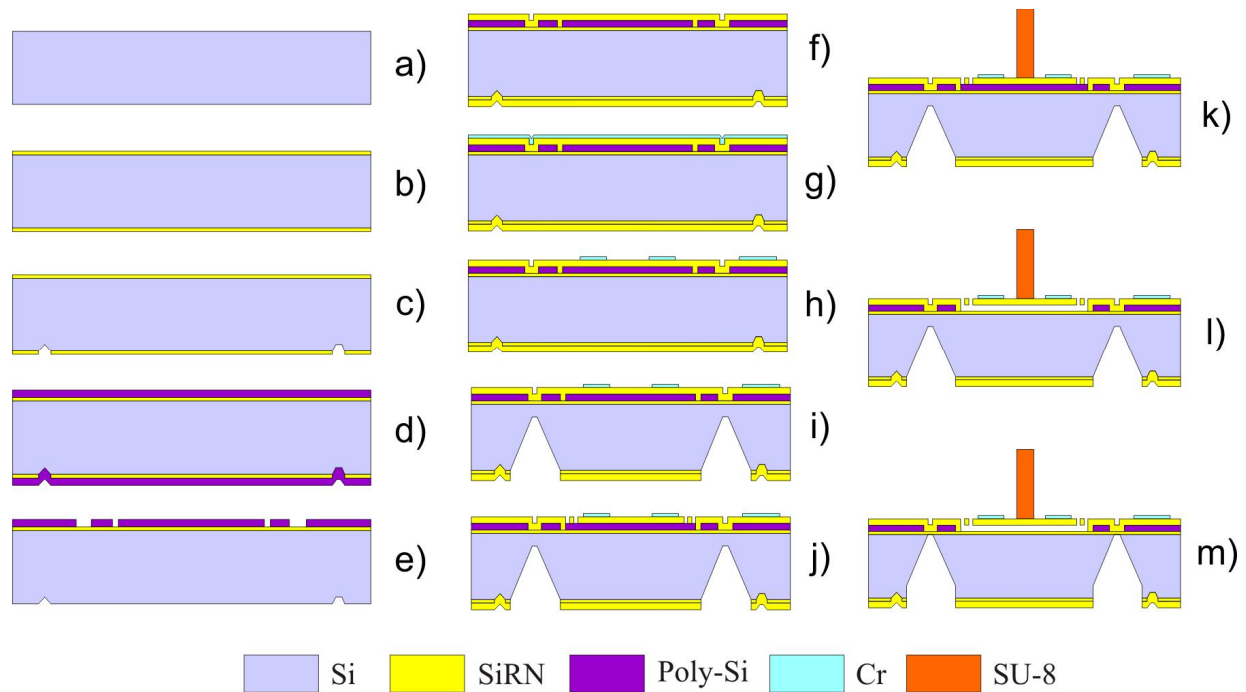

Fig. 8. Condensed process flow of the sensors. Fabrication is based on sacrificial use of poly-silicon to release siliconnitride membranes and the use of SU-8 for high aspect ratio hairs.

Next the front-side SRN layer is patterned to form the membranes and suspension springs (j). Two layers of 500 μm SU-8 photopolymer are spin-coated and exposed on the wafer surface to form the 1 mm long hairs (k). Processing is continued by dry etching of the sacrificial poly-silicon layer, thereby releasing the sensor structures, without affecting the SU-8 hairs (l). Finally a dry-RIE etch is applied to etch the last 50 μm of silicon. The structures are now readily broken out of the wafer producing elongated structures that can be assembled to form artificial cerci (figure 9) with 3D flow-measurement capability.
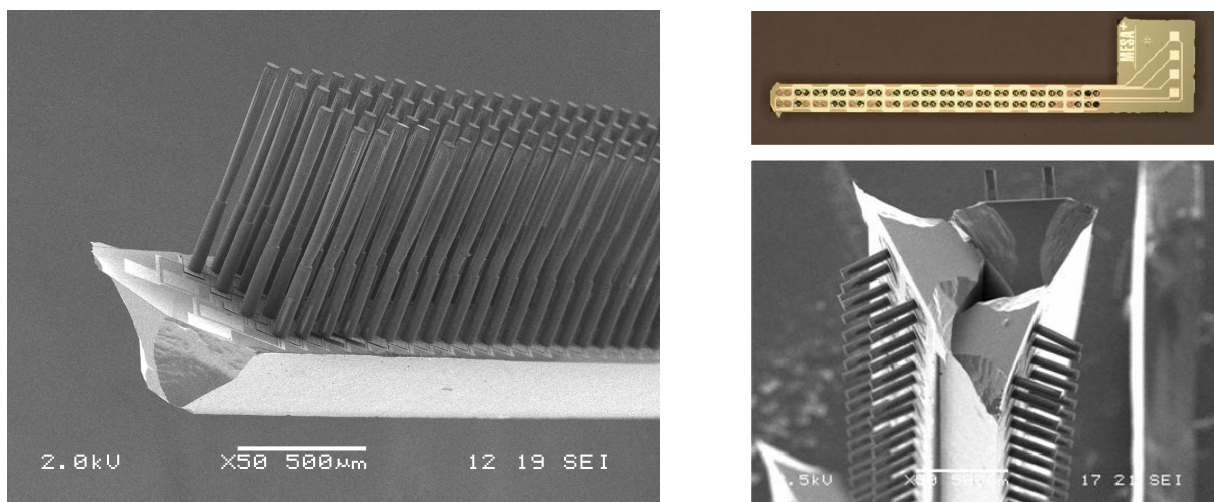

Fig. 9. Left: Array of about 1 mm long hairs. Right: modules which, when clued together, form an 'artificial cercus'.

4. CHARACTERISATION

Fabricated sensors were used for a variety of tests; they were investigated for structural characteristics by regular optical microscopy and White Light Interference Microscopy (WLIM) and observed by Laser Vibrometer (LV) when acoustically or electrostatically actuated to determine dynamic properties and to determine spring-softening effects.

4.1 Geometric characterization

During deposition of the silicon-nitride/chromium layer stack for the membrane intrinsic and thermal stress develops leading to upward curvature of the membrane. An example of the curvature present in the membranes is seen in figure 10 where a WLIM picture of a circular membrane is shown. Due to the semi-transparency of the membranes and the etching holes the profiles show some scatter as can be seen from the trace in the right picture. To estimate the deflection at the rim of the membrane a circle segment was fitted to the curve and the maximum deflection δ was estimated 2 µm. This deflection is relatively high when compared to the dielectric thickness of about 1.15 mm and has detrimental effects on both the sensitivity η and biasing constant κ.
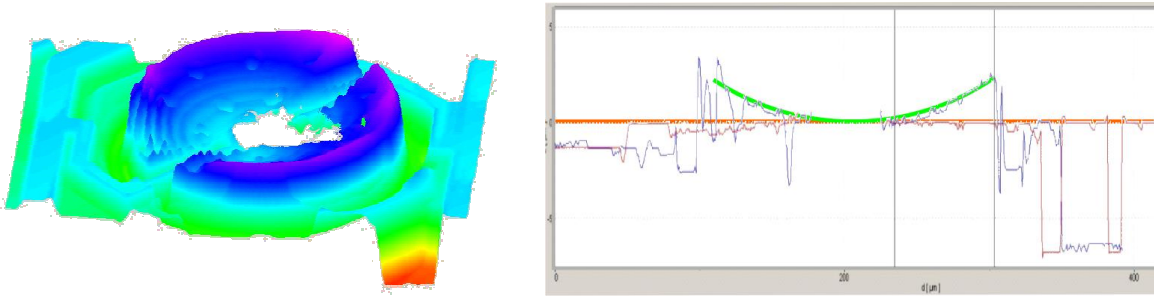

Fig. 10. Left: Whitelight Interference Micrograph of circular membrane showing significant curvature due to stress in the chromium/siliconnitride bilayer. Right: scanline through the membrane with circular approximation for the stress-induced deflection (green line).

4.2 Acoustic characterization

In a previous paper [16] we have shown acoustic characterization demonstrating acoustic sensitivity and figure-of-eight directional sensitivity. In that paper we used capacitive read-out demonstrating the viability of the concept. Here we present measurements on acoustic mechanical sensitivity by means of Laser Vibrometry (Polytec MSA400). These measurements give us the advantage of increased sensitivity and resolution and allow for direct observations of the acoustically induced tilt-angles, hence providing a means to compare measurements with aerodynamic-mechanical models. The measurement set-up is schematically shown in figure 11, left.
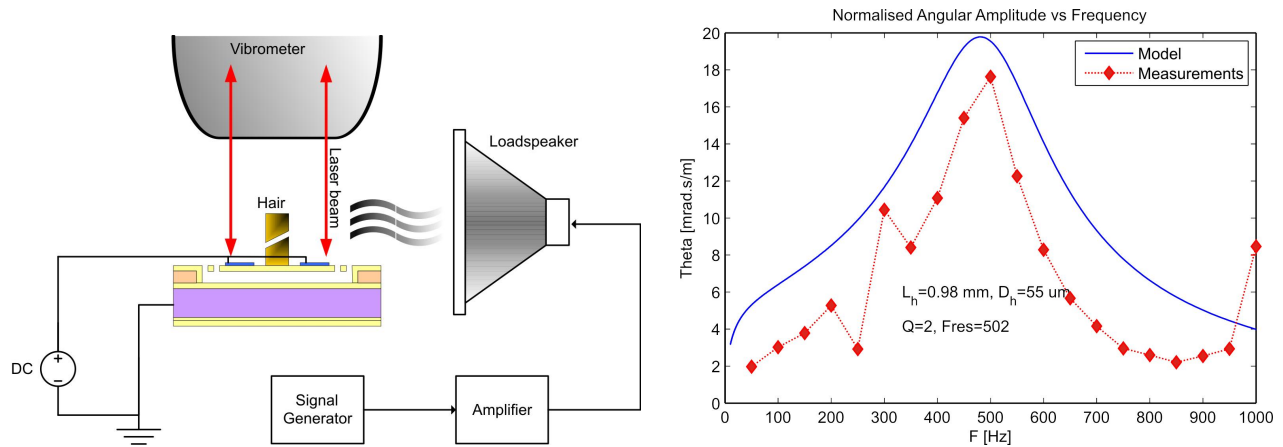

Fig. 11. Left: Schematic of measurement setup using a loudspeaker as very-near field sound source and the laser-vibrometer for detection of out-of-plane displacement at the rim of the membrane. Right: Angular rotation normalized to 1 m/s flow-velocity amplitude as obtained from the measurements and as predicted by the model.

The sensors are positioned under a scanning laser-vibrometer at a distance of a about $5-10$ mm from a square silicon plate ($\approx 2.5 \times 2.5$ cm^2) mounted on a loudspeaker. Since the distance of the hairs to the plate is so small, the loudspeaker induced particle velocity at the position of the hairs is in good approximation equal to the velocity of the loudspeaker itself. This so-called very-near field regime [17,18] exists at distances from the source smaller than the characteristic dimension of the sound source $L/2\pi$ and if L is much smaller than the wavelength λ. Since we are interested in relative low frequencies (< 1.0 kHz, $\lambda/2\pi > 5.4$ cm) the assumption of a very-near field source holds for distances of less than about 6 mm.

The scanning laser beam of the LV was adjusted to the rim of the membranes at the largest distance from the rotational axis. Since this distance was know, the displacements amplitudes were readily converted to angles of rotation which are comparable to the model predictions. The obtained rotational angles were divided by the velocity amplitudes of the silicon plate at given generator-signals and frequencies, measured separately with the LV. This yields the normalized angular rotation which is displayed as a function of frequency in figure 10 right. The model parameters were chosen in accordance to the device design and using readily available material properties as listed in Table 1. The only exception to this is the damping which was chosen to provide a quality factor of 2, roughly fitted to the experimentally observed transfer-function.

Comparison of the modeled and experimentally obtained data shows very satisfying similarity, not only qualitatively but also with respect to normalized rotation angles, hence giving the model credibility as well as the design optimizations derived from the model.

4.3 Biasing experiments

Two types of measurements were conducted on circular shaped sensors. Electrical actuation was used for determination of resonance frequencies at varying DC-biases and acoustic actuation was used for determination of air flow sensitivity versus DC-bias. In the latter case the experimental set-up was as given in figure 10 whereas in the former case the experiments were carried out without loudspeaker but with a combination of DC and AC voltages applied to one side of the membrane and DC voltage only applied on the other side.

Figure 12 left shows the measured resonance frequencies for the sensor at different applied DC-bias voltages when electrically actuated. The solid line is the relation as given in equation (14) fitted by a least squares fit to the measurement data for ω_{00} and κ/S. Clearly the model-dependence on U very well fits the experimental data. The resulting value for κ/S is 0.016 V^{-2} implying U_i=7.9 V.
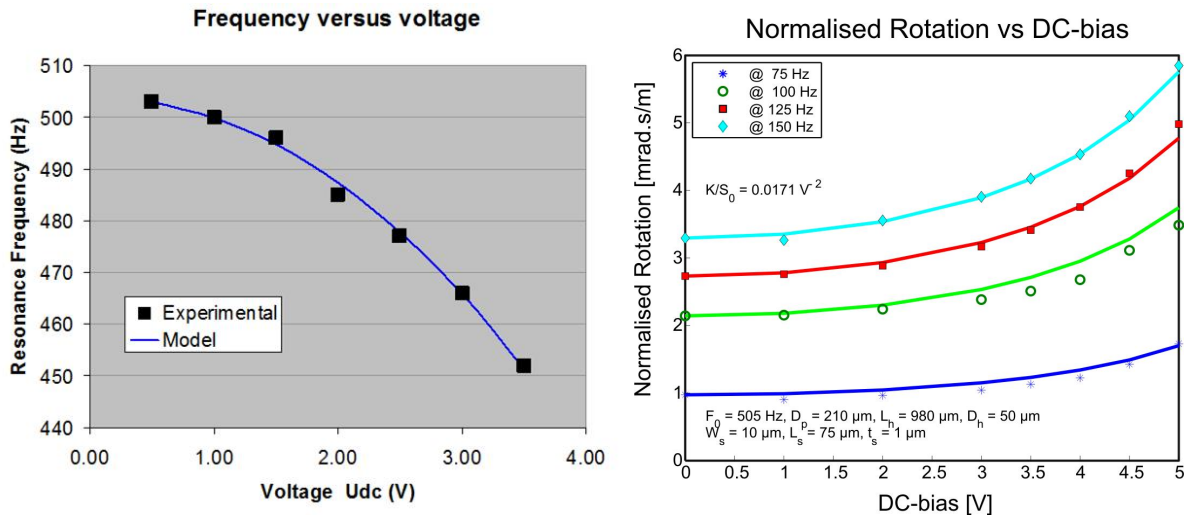

Fig. 12. Left: Resonance frequency versus DC-bias. Solid line is the model fitted (U_{bias}=0). Right: Normalized rotation of the membrane due to acoustically induced flow, vs. DC-bias. The model parameters are indicated in the figure.

Figure 12 right displays the measured membrane rotation amplitude normalized to the applied air flow from the loudspeaker versus the bias voltage at various actuation frequencies. Fitting the model equation (13) to all measurement

data using only one value $\kappa/S = 0.0171$ V^{-2} was found, quite close to the value obtained from the resonance frequency shift measurements. Again the model based predictions follow the experimental data quite close. As indicated in table 1 the calculated value of κ/S based on geometrical and material parameters only (i.e. without any fit) is 0.0156 V^{-2}, relatively close to the experimentally observed values.

5. DISCUSSION AND FUTURE RESEARCH

5.1 Model validity and device feasibility

The previous sections have shown that the theory developed as a framework for the understanding of flow-sensing in crickets by filliform hairs [11,12] is highly applicable to artificial hair-sensors. In comparison to crickets the structures made by MEMS technology seem rather well defined and also the materials parameters are mostly well-known. Moreover, more complicating effects like viscoelastic damping certainly occurring in the form of squeezed film damping in-between the capacitor plates, do not seem to obscure the physical first order effects, i.e. the second order nature of the artificial hair-sensors is clearly revealed in the experimental observations.
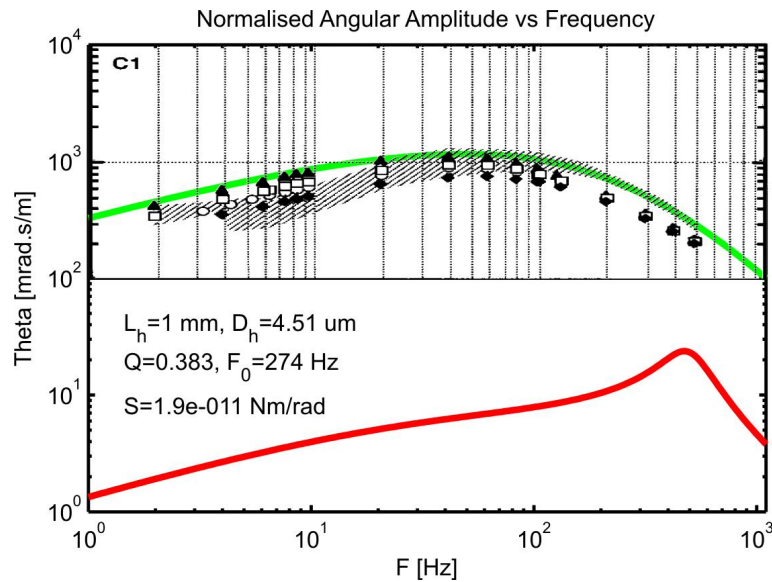

Fig. 13. Comparison of measured cricket hair-deflection response for hairs of length from 800 – 900 μm (markers) with model predicted response for cricket hairs (green line) and model predicted response for artificial hair-sensor design (red line). Data points taken from Shimozawa et al [11], model predictions based on the allometric scaling in [11]. Data is normalized to 1 m/s flow velocity amplitude.

What needs to be emphasized is that the sensitivity of the artificial sensors is about 2.3 orders of magnitude smaller than the hair-sensors of equal length in crickets hence rotation angles are much smaller implying that higher order effects are not easily observed. Looking at figure 13 it is clear that further optimization is required and as mentioned earlier the defined figure of merit gives clear directions for optimization with crickets scoring high with respect to this FOM.

5.2 Optimizing sensitivity

One of the attractive features of crickets' flow-sensitive hair-sensors is their high energy-sensitivity. In order for biomimetic hair-sensors to get to similar sensitivities much work still needs to be done.

Changing the drag-torque pick-up. The FOM introduced in section 2 shows that larger tilting angles at a usable bandwidth can only be obtained by using thin, long hairs, mounted on very compliant suspensions. This way the inertial moment is kept low while the drag-torque does not suffer considerably. For our sensory hairs this implies that we need to look carefully at increasing the aspect-ratio of the structures that we can make. The SU-8 currently used provides aspect ratios of about a factor of 10. Other shapes, e.g. by stacking two dissimilar parts, may partly resolve the problem. However, as far as mass-density goes, SU-8 is comparable in density at about $1.24 \cdot 10^3$ kg/m^3 [20] to the cuticle out of

which cricket hairs are made with a density of about $1.2 \cdot 10^3$ kg/m^3 [21]. Making hairs of comparable size with smaller inertial moment may potentially be achieved by using porous materials.

Towards flexible rotation. For drag-torques to produce large tilts evidently small rotational stiffness is required. However, in the current sensor design the torsion beams do not only provide angular compliance (S) but also have a limited stiffness (K) in vertical (x-direction in figure 3). The governing equations for S and K show that S is proportional to L^{-1} and K to L^{-3} where L is the length of the torsion beams. Hence on reducing S by increasing L, K will decrease faster than S. This has three detrimental effects: a) on decreasing K the voltage at which vertical pull-in occurs may become impractically low (since the capacitors are interrogated using voltages of about 1 V or more), b) low K-values may cause various stiction problems and c) in the dynamic response the resonance frequency of the vertical mode may get near the resonance frequency of the torsional mode causing unwanted mode-coupling.

Counteracting curvature. The curvature of the membranes has a detrimental effect on the sensitivity of the structures especially since it reduces the capacitance at positions farthest away from the rotational axis that contribute most to the sensitivity. Taking the values of table 1 and comparing η_C without curvature (= 9.0 pF/rad) to the value of η_C for a curvature with δ=2.0 μm (= 1.4 pF/rad) shows the importance of the effect. Hence it is important to reduce curvature significantly. If needed it can even be advantageous to reduce the chromium area near the rotational axis where it does not contribute significantly to sensitivity but does induce curvature [19]. Other options are the reinforcement of the silicon nitride membrane, the use of other electrode material, multi-layer stacks with stress compensation or structures incorporating stress-release mechanisms.

5.3 Interfacing

The sensors in the current devices are separated in two groups of sensors, all of the sensors in one group having the same directional orientation and being wired in parallel to obtain larger capacitances and capacitance variations. Hence, two groups with perpendicular directional sensitivity are formed. In first instance such a lay-out suffices for many experiments needed to characterize the sensors. However, as mentioned in the introduction, eventually the potential of these types of sensors is to measure flow-patterns with high areal density rather than single flow observations. To this end the sensors need to be interrogated individually. One way to do so is illustrated in figure 14. In this architecture a bank of oscillators is applied to feed signals to each of the columns of sensors. Along the rows the signals are collected and transported off-chip. By multiplying the summarized output with the same range of frequencies used in the oscillator bank, e.g. in a signal processor based system, the information of all individual sensors can be retrieved. Such a system would open-up possibilities to measure, characterize, categorize and eventually recognize specific amplitude / frequency / spatial flow signatures.
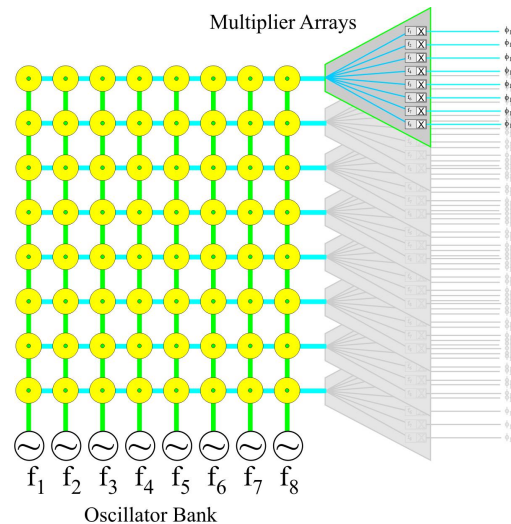

Fig. 14 Possible architecture for multiple access on individual hairsensors.

6. CONCLUSIONS

Biomimetic hair-sensor arrays for determination of AC flows and flow-patterns, based on flow-sensitive hair-sensors found on crickets have been proposed. The analysis and fabrication has been described and experimental results using Laser Vibrometry and White Light Interference Microscopy are presented. It was shown theoretically and experimentally that these sensors can be adaptively and reversibly changed by applying a DC-bias on the electrodes forming the capacitors used for read-out. The current device-design has been analyzed and a Figure Of Merit quantifying the usability of these sensors has been introduced. Using this FOM the artificial sensors were compared against there biological source of inspiration and found to lack behind by almost two orders of magnitude. Based on these findings possible routes for further optimization of sensitivity have been identified for future research.

REFERENCES

1. Gijs J M Krijnen et al, Nanotechnology, vol 17, pp. 84-89, 2006
2. K. Snyder et. al, F. Sachs, W. Brownell, Chapter 6 in "Sensors and Sensing in Biology and Engineering", ed. Barth, Humphry and Secomb (Springer) Vienna, 2003.
3. T. Wellens, V. Shatokhin and A. Buchleitner, Rep. Prog. Phys. 67, 2004.
4. J. Levin, J. Miller, Nature, Vol 380, 1996, 165-168.
5. S. Bahar, F. Moss, Mathematical Biosciences Vol. 188, 2004, 81–97.
6. T. Shimozawa, J. Murakami, T. Kumagai, Chapter 10 in "Sensors and Sensing in Biology and Engineering", ed. Barth, Humphry and Secomb (Springer), Vienna, 2003.
7. C. Magal, O. Dangles, P. Caparroy, J. Casas, Journal of Theoretical Biology 241 (2006) 459–466
8. Landolfa M.A. and Jacobs G.A. Journal of Comparitive Physiology A 177, 1995, 759-766
9. J. Tautz, Naturwissenschaften, Vol 66, 1979, p.452-461.
10. F.G. Barth, Cur. Opinion in Neurobiology, Vol-14, 2004, 415-422.
11. S. Coombs, Autonomous Robots 11, 2001, 255-261.
12. J. van Honschoten, V. Svetovoy, G. Krijnen, M. Elwenspoek, J. of Microelectromech. Syst. 14, 2005, pp. 436-443
13. T. Shimozawa, T. Kumagai, Y. Baba, Journal of Comparative Physiology A 183, 171-186
14. J.A.C. Humphrey, et al. Philosophical Transactions: Biological Science 340, 423-444
15. J.G.E Gardeniers et al., J. Vac. Sci. Technol. A, 1996, 14, (5), pp. 2879–2892.
16. Dijkstra et. al, J. Micromech. Microeng. 15 (2005) S132–S138.
17. H-E. de Bree, V.B. Svetovoy, R. Raangs, R. Visser, 11th Int. Cong. on Sound and Vibration (ICSV11), St. Petersburg 2004.
18. R. Raangs, PhD thesis, Univ. of Twente, Enschede, The Netherlands, 2005.
19. N. Izadi, R. K. Jaganatharaja, J. Floris and G. Krijnen, accepted for presentation at the DTIP 2007 conference, 25-27 April 2007, Stresa, Lago Maggiore, Italy.
20. MicroChem company SU-8 data-sheets
   http://www.microchem.com/products/pdf/SU-82000DataSheet2100and2150Ver5.pdf
21. Jensen M, Weiss-Fogh T, Philos Trans R Soc Lond B, Vol 245, 1962, pg 137 - 163